Applied Thermal Engineering 181 (2020) 116044

Contents lists available at ScienceDirect

Applied Thermal Engineering

journal homepage: www.elsevier.com/locate/apthermeng

Effects of copper oxide and sulfuric acid on the pyrolysis behavior of ammonium nitrate under thermal radiation experiments

Qi Sun [a], Lin Jiang [b], Huiqi Cao [c], Jinhua Sun [c,*], Ganbin Liu [a]

[a] School of Civil and Environmental Engineering, Ningbo University, Ningbo, Zhejiang 315211, China
[b] Department of Mechanical Engineering, Nanjing University of Science and Technology, Nanjing, Jiangsu 210094, China
[c] State Key Laboratory of Fire Science, University of Science and Technology of China, Hefei, Anhui 230027, China

ARTICLE INFO

Keywords:
Ammonium nitrate
Thermal radiation
Mass loss rate
Pyrolysis behavior
Emergency response

ABSTRACT

Statistics have indicated that industrial accidents of ammonium nitrate were primarily caused by uncontrolled external fires where heating was dominantly controlled by radiation, and yet existing studies at milligram scale cannot fully simulate the real fire scenarios. To explore the pyrolysis behavior in typical fires, this study conducted thermal radiation experiments using pure ammonium nitrate, and its mixtures with copper oxide and sulfuric acid. Different from the pyrolysis process identified in milligram scale tests, the bench-scale pyrolysis of ammonium nitrate under radiation consisted of four stages. Pyrolysis structure model of each stage was built to reveal the differences in dominated thermal behavior. Results indicated that two additives had different thermochemical effects on pyrolysis of ammonium nitrate. Sulfuric acid accelerated the reaction rate of each stage by generating catalytic nitric acid; copper oxide reduced the number of reaction stages into three via surface absorptions. The time and mass loss rate of different stages were determined. Recommendations on effective emergency response were made to prevent the transition of slow decomposition into fast decomposition, and thus to intervene the fire-induced domino effect of ammonium nitrate. This study helps to understand the pyrolysis behavior of ammonium nitrate under fire exposure, and provides insights for pyrolysis modeling and firefighting in industry of interest.

1. Introduction

Ammonium nitrate (AN) is one of the most widely known hazardous chemicals. It is generally used as the nutrient in agricultural fertilizers and the oxidizer in explosives [1,2] for the advantages compared with other oxidizers, including low cost, easy availability, strong gas generation, chlorine free combustion nature and so on [3]. As an important green oxidizer [4] and a commonly used commercial product, AN is playing an increasingly important role in the development of eco-friendly solid fuels. However, the inherent thermal instability of AN often leads to fire and explosion accidents during storage and transport.

A number of studies related to hazards of AN and mixtures under elevated temperature have been published. According to Marlair and Kordek [5], the thermal hazards of AN are threefold, including fire hazard, thermal decomposition hazard, and explosion hazard. One major safety problem of AN is that it melts and decomposes when heated over 170 °C. Studying the thermal stability of AN and effects of additives has been a popular topic for many years [6]. Recently, Babrauskas and Leggett [1] published so far the most extensive and complete review related to thermal hazards of AN. According to the review, applying thermal analysis techniques (e.g. TGA, DSC, C80) to study the decomposition of milligram AN substances in inert or oxidizing atmosphere, and at various heating rates, has become a fundamental procedure. Through a series of data processing, thermal runaway hazards of AN were generally described by onset decomposition temperature, heat of reaction, activation energy, pressure release rate, mass loss and so on [6–14]. It is widely accepted that AN has a single pyrolysis stage under elevated temperature.

However, AN related thermal behaviors are much complicated in real fire accidents. Oxley et al. [8] summarized seven typical patterns including, blast → explode, fire → explode, fire no explode, thermal runaway → fire → no explode, thermal runaway → detonation, fire → blast → detonation and blast no detonation. Similarly, Babrauskas [15] reviewed the AN related explosions throughout a century and found that 100% of AN's explosion accidents in storage or transport had a single causative factor, the uncontrolled external fire. For instance, the catastrophic fire and explosion accidents that occurred at Tianjin Port, China

* Corresponding author.
E-mail address: sunjh@ustc.edu.cn (J. Sun).

https://doi.org/10.1016/j.applthermaleng.2020.116044
Received 18 December 2019; Received in revised form 7 September 2020; Accepted 9 September 2020
Available online 14 September 2020
1359-4311/

Nomenclature

MLR (g s^{-1})	Mass Loss Rate
MLR_I (g s^{-1})	Mass Loss Rate at the end of stage I
MLR_{II} (g s^{-1})	Mass Loss Rate at the end of stage II
MLR_{max} (g s^{-1})	Mass Loss Rate at the end of stage III (the maximum mass loss rate)
t_I (s)	Time at the end of stage I
t_{II} (s)	Time at the end of stage II
t_{max} (s)	Time at the end of stage III (time at the maximum mass loss rate)
t_{end} (s)	Time at the end of stage IV (total time of pyrolysis process)
ISO	International Standardization Organization
AN	Ammonium Nitrate
CuO	Copper Oxide
H_2SO_4	Sulfuric Acid
C80	C80 Micro Calorimeter
DSC	Differential Scanning Calorimetry
TG	Thermogravimetry
XRD	X-Ray Diffraction
IR	Infrared Radiation
SEM	Scanning Electron Microscope
R	Reaction
l	Liquid
s	Solid
g	Gas

in 2015 [16,17] followed this pattern. The initial fire was caused by the self-ignition of nitrocellulose, and yet the large amount of AN acting as both explosives and strong oxidizers strongly supported the evolution of fire and caused pronounced fires and explosions, killing 165 people. The role of AN here is a typical fire-induced domino effect, which combines an uncertain event (the primary fire accident of nitrocellulose) and deterministic events (the secondary fire and explosion accidents of AN) [18]. As a low-frequency high consequence chain of accidents, the primary threat of domino effect is that the consequences of secondary accidents are much more severer than the consequence of the primary accident [19,20].

The Tianjin Port accident has drawn high attention from researchers to consider adopting new methodologies and perspectives to study the thermal behavior of hazardous chemicals [21]. Existing findings through milligram scale experiments may not provide sufficient information to describe the thermal process of AN and mixtures in real fire, or to support emergency responses in industrial accidents. Babrauskas and Leggett's review [1] also highlighted that, most of the explosions of AN involved fire as the proximate cause, and yet there are limited studies that heating AN by fire radiation or to explore the firefighting of AN in fire. A relevant work by Han et al. [22] studied the capability and complications when using water to extinguish fires involving AN stock, and proposed the mechanism for thermal decomposition developing to detonation. As one of the few articles, this paper emphasized that AN fire is a thermal process that differs from normal combustions due to the complicated physical and chemical characteristics [22]. The chemical mechanism during decomposition of AN in milligram scale has been widely discussed, and yet limited studies analyze the chemicals in bench scale with fire radiation dominated heating.

This paper applies a Desktop Cone Heating Apparatus (DCHA) to simulate the fire radiation-controlled heating scenario, and measures the mass loss rate (MLR) to characterize the pyrolysis behavior of AN and mixtures exposed to radiation in different intensities. Among varied additives, two catalysts, copper oxide (CuO) and sulfuric acid (H_2SO_4) are selected. H_2SO_4 is a common chemical contaminant in the manufacture, storage, transportation and use of AN [6,23]. According to the C80 micro calorimetric studies conducted by Sun et al. [23], H_2SO_4 catalyzes the thermal decomposition of AN by greatly reducing the initial temperature. CuO is an important phase stabilization source for AN. Several studies [6,24–26] have investigated the influence of CuO on thermal decomposition related hazards of AN through micro calorimeter techniques. However, the pyrolysis behaviors when AN was mixed with either CuO or H_2SO_4 have not been studied, which are necessary for the safe use of AN in industry. This study aims to explore the pyrolysis behavior of AN under different radiant fluxes, and the effects of additives on pyrolysis behavior of AN. Findings of this study will provide useful insights for the optimal use of AN as important sustainable energy resources, and will also contribute to the development of appropriate fire detection and firefighting technologies to effectively ensure the safety application of AN and mixtures in industries of interest.

2. Material and experiments

Three materials are applied in this study. The pure AN (> 99%) was purchased from Beijing Lantai Chemical Technology co., Ltd. The AR grade CuO was purchased from Aladdin (Shanghai) co., Ltd. The AR grade concentrated H_2SO_4 was purchased from Sinopharm Chemical Reagent co., Ltd. Due to the hygroscopicity of AN, mechanical lapping was applied to polish the crystal of AN. The grinded AN samples with uniform particle sizes were placed in a vacuum drying chamber at 55 °C for 24 h to eliminate the potential interference of moisture. The AR grade CuO samples were sealed and stored in confined place to keep dry.

The thermal radiation experiments were performed through a DCHA, as shown in Fig. 1(a). It consists of a cone heater, a radiation controller with a temperature panel, an electronic balance, a stainless sample holder, a camera, a computer and an exhaust fume collecting hood with connection to the ventilation system. The cone heater and radiation controller were provided by Suzhou Yangyi Vouch Testing Technology Company, China. The cone heater was built in accordance to the ISO 5660.1 [27,28], which has been applied by fire safety scientists to study the pyrolysis of biomass [29–31], polymers [32,33] and construction materials [27,34–36] for many years. DCHA allows to set radiation heating scenarios with heat flux of 0 ~ 100 kW m^{-2} via the radiation controller. The electricity requirement for the radiation controller is 220 V (alternating voltage), 6 KVA with electric leakage. Two pieces of fan-shaped thermal baffle made by asbestos were placed at the bottom of the cone heater during pre-heating to isolate samples from radiation. Pyrolysis experiments started after the temperature (heat flow) was kept stable for 3 min. A Mettler Toledo XP10002S electronic balance with data acquisition of 0.01 g was applied to measure the mass loss of samples under thermal radiation. The experiments were recorded with a camera and connected to a computer for real-time observation. Note that the measurement of MLR through DCHA is consistent with Cone Calorimeter, but the cost of DCHA is much lower (about 1700 $ for both cone heater and the radiation controller).

The sample holder of AN was set as a cuboid with dimension of 60 × 60 mm to create a two-dimensional heating scenario [27,37]. AN with mass of 30, 50 and 80 g were horizontally spread on the sample holder and heated under certain radiation flux. The sample holder was height-adjustable to ensure that the distance from materials' top surface to the bottom of radiation heater was kept constant. Three typical radiant fluxes in fire (25, 35 and 50 kW m^{-2}) were selected for experiments [37]. The corresponding temperatures of the radiation controller were around 660 °C, 735 °C and 820 °C, respectively with an error of 2 K. The experimental procedure is presented with a flowchart of Fig. 1(b). Please note that the DCHA also allows the ignition of materials through a 10 kV ignition needle and the radiation controller, which was not emphasized in the current study. In addition to the DCHA, this study also applied an

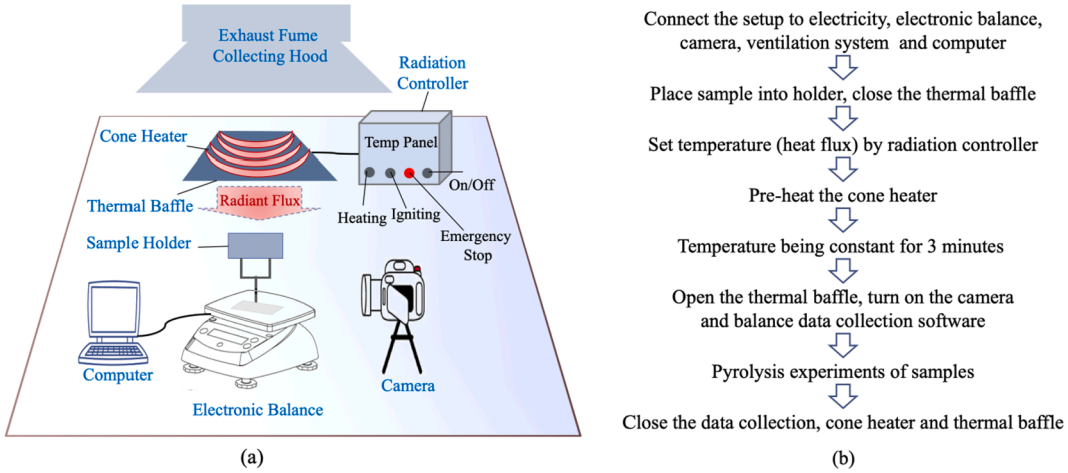

Fig. 1. (a) A schematic diagram of the Desktop Cone Heating Apparatus (DCHA) ; (b) A flowchart of the experimental procedure applied in this study.

automatic sample grinding machine to mechanically mix AN and CuO (using ceramic beads at frequency of 15 HZ for 90 s), as well as a GeminiSEM 500 to capture the micro surface of AN/CuO mixture.

Table 1 summarizes the sample information and corresponding radiant fluxes of 18 sets of experiments conducted in this study. Please note that the order of number in the first column is consistent with the order of sample information, e.g. No.2 referring to the experiment with 50 g AN. Before each test, the mixtures containing 6 wt% H_2SO_4 were made by adding 2 mL of liquid into dried AN (30 g) and slowly stirred in an incubator; the AN-CuO samples were manually mixed in a sealed glass bottle using dried AN and certain amount of dried CuO. Since the samples were in shape of crystal particles, it was assumed that the involvement of either CuO or H_2SO_4 would not change the thickness of the sample. Each experiment was duplicated twice to ensure the repeatability. The uncertainty and error of this study has two major sources, the digital instruments of DCHA and the uncertainty propagation in calculations. For the errors in digital instruments, the cone heater delivers an error of 10 % according to the Cone Calorimeter which applies the same cone heater [38]. The balance has a readability of 0.01 g with capacity of 10,100 g, and thus the error of balance can be ignored with sample mass of 30 g, 50 g and 80 g. The calculation uncertainty is mainly caused by the smoothing of *MLR* with Stavitzky-Golay method, which will be introduced in Section 3.

3. Results and analysis

3.1. Pyrolysis behavior of pure AN under thermal radiation

Numerous thermal decomposition experiments have been conducted using pure AN [1,7]. Despite the variety in applied apparatus and heating procedures, the mass loss always has a single stage when the sample with limited size were uniformly heated during the entire decomposition process. However, the pyrolysis behavior of AN under thermal radiation experiments was found to be different. In the current study, nine sets of experiments (1 ~ 3, 7 ~ 9 and 13 ~ 15) were conducted using pure AN under three radiant fluxes. As an example, Fig. 2 (a) presents the mass loss (the black blocks) and *MLR* (the black line curve) profiles of 80 g AN under 50 kW m^{-2}, corresponding to experiment No.15. The *MLR* in unit of g s^{-1} was calculated as the first-order derivative of time and then smoothed by the Stavitzky-Golay method (the red point curve) [39]. According to the camera, once exposed to radiation, AN started to lose mass and was completely decomposed before 500 s. The entire decomposition process released a lot of smoke, and no flame was observed.

From the smoothed *MLR*, the pyrolysis process of AN consisted of four regimes, noted as stage I ~ IV in Fig. 2 (a). This is different from the evolution of mass loss stage in TG [7], indicating the complicated heat and mass transfer mechanism when AN in certain thickness was exposed to radiation. From 0 s to 116 s, the *MLR* of AN gradually increased, corresponding to the stage I. Then the value of *MLR* did not change much for about 120 s, referring to the stage II. In these two stages, AN melted and decomposed slowly, noted as the slow decomposition period. The melting behavior was not clearly reflected by either mass or *MLR*, because the pyrolysis process was very fast. Then *MLR* started to increase rapidly in the stage III, and reached the MLR_{max} with total sample mass reduced from 80 g to about 30 g. This corresponds to the fast decomposition period. Finally, *MLR* reduced to zero before 600 s and AN was fully decomposed, corresponding to the stage IV, i.e. the decay period.

The aforementioned data processing methodology was applied to all sets of experiments. The results are presented in Fig. 3. The same four-stage evolution characteristic was identified among all samples. An exception was that the values of MLR_{II} were slightly larger than that of MLR_I for No. 3, 8, 9, and 15. This is probably due to the complicated heat and mass transfer inside materials with larger sample mass. Overall, the increase rates of *MLR*s in stage II were much slower than that in stage I and III. Despite the differences in sample mass and radiant flux, the *MLR* evolution of AN during pyrolysis consisted of four stages, in which the *MLR* was slowly increasing (stage I), being steady (stage II), rapidly increasing to MLR_{max} (stage III) and reducing to zero (stage IV), respectively. In stage I and II, AN decomposed relatively slow, noted as the slow decomposition period. Stage III and IV referred to the fast decomposition period and decay period, respectively.

In order to quantitatively characterize the pyrolysis process, seven parameters are defined in this paper, as marked in Fig. 2. The terms of t_I, t_{II}, t_{max} and t_{end} (s) refer to the time at the end of stage I, II, III and IV, respectively. The terms of MLR_I, MLR_{II} and MLR_{max} (g s^{-1}) refer to the value of *MLR* corresponding to the end of stage I, II and III, respectively. The seven parameters of pure AN are listed in Table 2, in accordance to

Table 1
Summary of the sample information and radiant flux.

No.	AN (g)	CuO (wt.%)	H_2SO_4 (wt.%)	Radiant Flux (kW m^{-2})
1, 2, 3	30, 50, 80	0	0	25
4, 5	30	5, 10	0	25
6	30	0	6	25
7, 8, 9	30, 50, 80	0	0	35
10, 11	30	5, 10	0	35
12	30	0	6	35
13, 14, 15	30, 50, 80	0	0	50
16, 17	30	5, 10	0	50
18	30	0	6	50

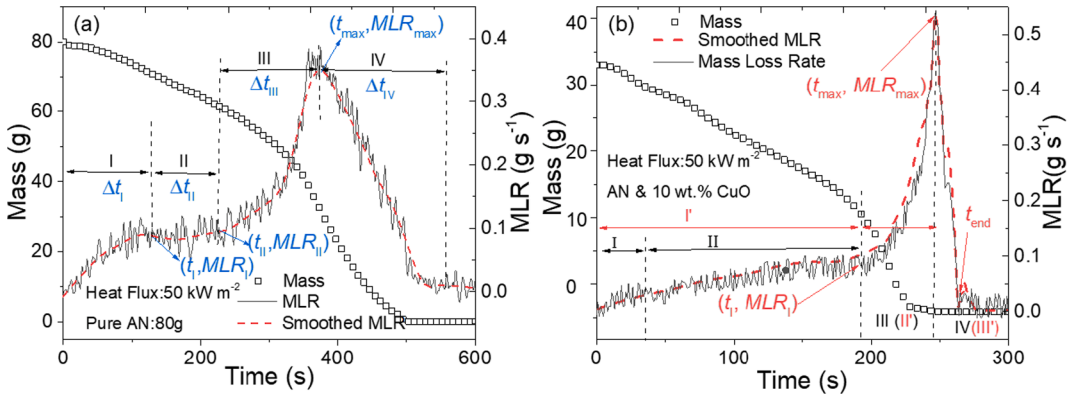

Fig. 2. The pyrolysis stages (I ~ IV) of (a) pure AN, and (b) AN mixed with 10 wt% CuO under radiant flux of 50 kW m^{-2}.

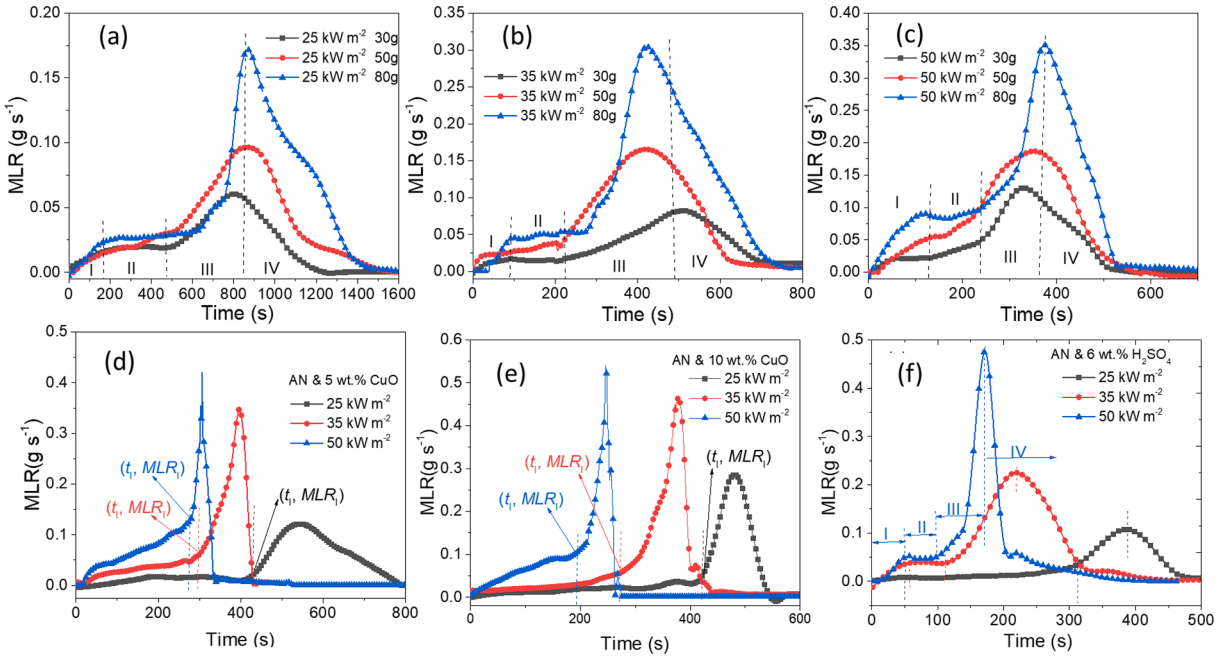

Fig. 3. The pyrolysis stages of, AN under radiant flux of (a) 25 kW m^{-2}, (b) 35 kW m^{-2} and (c) 50 kW m^{-2}; and AN mixed with (d) 5 wt% CuO, (e) 10 wt% CuO and (f) 6 wt% H_2SO_4 under three radiant fluxes.

No. 1 ~ 3, 7 ~ 9 and 13 ~ 15, respectively. The order of number is consistent with the experimental information listed in Table 1. These parameters quantitatively indicate how the pyrolysis process of AN was evolved with change of sample mass, radiant flux and radiation time. Please note that the *MLR* data in Table 2 are limited to two decimal places because the readability of balance is 0.01 g. The experimental uncertainties of *MLR* are computed as two standard deviations of the mean.

It can be seen from Table 2 that, under a certain radiant flux, the t_{max} values of samples in different masses were close to each other, indicating the reliability of the experiment. The time corresponding to each decomposition stage is roughly described by a time region as follows. When AN was exposed to radiant flux of 25 kW m^{-2}, the time period of stage I (t_I), II ($t_I \sim t_{II}$), III ($t_{II} \sim t_{max}$) and IV ($t_{max} \sim t_{end}$) was in the region of 0 ~ 200 s, 200 ~ 500 s, 500 ~ 900 s and 900 ~ 1500 s, respectively; the t_{max} was at about 800 ~ 900 s. Similarly, when AN was exposed to radiant flux of 35 kW m^{-2}, the time of stage I, II, III and IV was in the region of 0 ~ 100 s, 100 ~ 230 s, 230 ~ 500 s and 500 ~ 800 s, respectively; the t_{max} was in the region of 400 ~ 500 s. At 50 kW m^{-2}, the time of four pyrolysis stages was in 0 ~ 120 s, 120 ~ 240 s, 240 ~ 380 s and 380 ~ 600 s, respectively; and the t_{max} was in the region of 300 ~ 400 s. Besides, a larger sample mass led to higher MLR_{max}. For example, with mass increasing from 30 g to 80 g, the MLR_{max} increased by nearly 2.7 times at 35 kW m^{-2}. This indicated that a larger accumulation mass mainly acted on the fast decomposition period, i.e. the stage III.

For the effects of radiant flux, it is obvious that a larger radiant flux could accelerate the entire pyrolysis process by reducing the time of each stage and increasing the t_{max}. Taking the case with 80 g AN as an example, when the radiant flux was increased from 25 kW m^{-2} (No. 3) to 50 kW m^{-2} (No. 15), the t_{max} increased twice (500 s), the MLR_{max} reduced by over a half; and the value of t_{end} was also reduced by over a half (900 s). The same change fashion was observed for the cases with mass of 30 g and 50 g. Since the time region of pyrolysis stages was directly linked to radiant flux, the statistical data from Table 2 could be used as reference data for emergency response planning when pure AN is exposed to external fire. For example, if the thermal radiation of external fire was expected to be about 50 kW m^{-2}, effective firefighting strategies such as cooling and thermal insulation should be adopted before 380 s to prevent AN from rapid decomposition. Detailed discussions about this topic are available in Section 3.4.

Table 2
Summary of the quantitative characterization parameters of all tests.

No.	t_I (s)	MLR_I (g s^{-1})	t_{II} (s)	MLR_{II} (g s^{-1})	t_{max} (s)	MLR_{max} (g s^{-1})	t_{end} (s)
1	247	0.02 ± 4.6%	472	0.02 ± 2.3%	804	0.06 ± 6.9%	1300
2	270	0.02 ± 3.9%	310	0.02 ± 2.3%	864	0.10 ± 8.1%	1500
3	257	0.03 ± 5.2%	620	0.03 ± 3.0%	874	0.17 ± 5.0%	1500
4	400	0.01 ± 3.0%	N/A	N/A	548	0.12 ± 4.1%	800
5	394	0.03 ± 4.2%	N/A	N/A	482	0.29 ± 8.4%	600
6	51	0.01 ± 1.0%	130	0.01 ± 6.2%	374	0.11 ± 6.6%	500
7	90	0.02 ± 2.2%	223	0.02 ± 1.5%	505	0.08 ± 4.9%	1100
8	45	0.02 ± 5.3%	215	0.04 ± 4.0%	424	0.17 ± 3.0%	1100
9	96	0.05 ± 4.2%	279	0.06 ± 2.8%	422	0.30 ± 3.7%	900
10	270	0.05 ± 2.9%	N/A	N/A	397	0.35 ± 6.8%	500
11	277	0.05 ± 2.3%	N/A	N/A	380	0.46 ± 3.6%	500
12	60	0.04 ± 4.5%	118	0.04 ± 2.9%	220	0.23 ± 5.1%	400
13	58	0.02 ± 2.0%	117	0.02 ± 3.2%	335	0.13 ± 2.5%	600
14	137	0.06 ± 4.6%	167	0.06 ± 2.9%	357	0.19 ± 8.3%	700
15	116	0.09 ± 3.5%	236	0.10 ± 1.5%	373	0.35 ± 5.8%	600
16	278	0.13 ± 2.1%	N/A	N/A	307	0.42 ± 6.8%	400
17	178	0.09 ± 3.5%	N/A	N/A	246	0.54 ± 4.9%	300
18	56	0.05 ± 1.5%	100	0.05 ± 2.9%	172	0.48 ± 3.8%	300

3.2. Pyrolysis behavior of AN mixtures under thermal radiation

Two typical additives were added to AN to explore their effects on the pyrolysis behavior of AN. The effect of CuO was studied by adding 5 wt% and 10 wt% CuO to AN and exposing the mixtures to radiant flux of 25 kW m^{-2}, 35 kW m^{-2} and 50 kW m^{-2}, respectively. The same data processing methodology mentioned in Section 3.1 was applied for analysis. The results are shown in Fig. 2 (b). Since CuO did not participate in the mass loss process due to the catalytic effects [6,24–26], the original mass of CuO was subtracted from the total mass of mixture before processing the data. Similar to pure AN, once exposed to thermal radiation, the AN/CuO mixtures started to loss mass for about 250 s till all of the AN samples were decomposed into gases. A large amount of gas was released during the whole pyrolysis process, and no flame was observed.

Comparing to the *MLR* profile in Fig. 2 (a), the major difference in Fig. 2 (b) is that the aforementioned four-stage evolution characteristic was reduced into three stages. This is also different from the mass loss process of AN/CuO observed by TG experiments. In the slow decomposition period, the *MLR* continuously increased with a steady increase rate and finally reached $MLR_{I/II}$ of 0.09(±3.5%) g s^{-1} at 178 s. Then in the fast decomposition period, the increase rate of *MLR* became larger; *MLR* quickly reached the MLR_{max} of 0.54(±4.9%) g s^{-1} at 246 s, and then reduced to 0 before 300 s. The detailed time and *MLR* values of each stage are summarized in Table 2 (No. 17). Comparing to pure AN with the same mass under the same radiant flux (No.13), the t_{max} was reduced by one third, the total pyrolysis time was 50% shorter, and the MLR_{max} increased by four times. This indicates that the involvement of CuO could accelerate the entire pyrolysis process by merging the first two slow decomposition stages and significantly enhancing the reaction rate in the fast decomposition period. The same three-stage evolution characteristic of *MLR*s was observed among AN/CuO mixtures with other mass proportions under other radiant fluxes, as shown in Fig. 3 (d) ~ (e). The boundaries of stage I and II for each curve were marked with a dash line. The detailed values of t_I, MLR_I, t_{max}, MLR_{max} and t_{end} are all listed in Table 2, corresponding to No. 4 ~ 5, 10 ~ 11 and 16 ~ 17.

From Fig. 3 and Table 2, the catalytic effects of CuO depended on both mass proportion in the mixture and the external radiant flux. Firstly, the larger the mass proportion, the shorter time required by AN to reach a higher MLR_{max}. For example, when proportion of CuO was increased from 5 wt% to 10 wt% at 50 kW m^{-2}, the t_I reduced by one third, the t_{end} reduced by a quarter, and the MLR_{max} increased with a sharper peak in profile. Secondly, the effects of thermal radiation were primarily presented by the time reduction in each pyrolysis stage, as well as the increase of MLR_{max}. In Fig. 3 (d), both t_{max} and t_{end} reduced approximately half when radiant flux was increased from 25 to 50 kW m^{-2}, while the MLR_{max} increased by nearly 2.5 times. The same fashion was shown in Fig. 3 (e) where the *MLR* profile became much sharper under a higher radiant flux, indicating the dramatic catalytic effects of CuO on pyrolysis of AN.

The effects of H_2SO_4 on pyrolysis of AN were studied by adding 2 mL concentrated H_2SO_4 to AN and exposing the mixtures to three radiant fluxes. Similarly, mass of the AN/H_2SO_4 mixture started to reduce continuously once the experiments started, as presented in Fig. 3 (f). The pyrolysis process ended before 500 s, 400 s and 300 s under 25 kW m^{-2}, 35 kW m^{-2} and 50 kW m^{-2}, respectively. Different from AN/CuO mixtures which had certain amount of final residue (the unreacted CuO), both AN and H_2SO_4 were fully decomposed into gases. Besides, the entire pyrolysis process released a large amount of smoke and no flame was observed.

The same data processing methodology was applied to handle the mass loss data of AN/H_2SO_4 mixtures. Same as the four pyrolysis stages of pure AN, the evaluation of *MLR*s also consisted of four stages in which the mixture increased slowly, being stable, increased rapidly and decreased to zero. The values of t_I, MLR_I, t_{II}, MLR_{II}, t_{max}, MLR_{max} and t_{end} are summarized in Table 2, corresponding to No. 6, 12 and 18, respectively. Comparing to pure AN with the same mass (No. 1, 7 and 13), the involvement of H_2SO_4 did not change the pyrolysis stages, but significantly accelerated the decomposition rates. In other words, H_2SO_4 participated in the pyrolysis by chemical decomposition reactions and was fully decomposed. Under radiant flux of 25 kW m^{-2}, the involvement of H_2SO_4 reduced both t_{max} and t_{end} by more than 50%, and doubled the MLR_{max}. The same fashion was shown with the cases under other two radiant fluxes. For the effects of radiation, the *MLR* profile at 50 kW m^{-2} showed a much sharper peak, and t_{max} was 200 s earlier than that of 25 kW m^{-2}. Comparing Fig. 3 (d)~(e) to Fig. 3 (f), although both CuO and H_2SO_4 significantly accelerated the pyrolysis of AN, the *MLR* profiles were in different shapes, especially under the condition of high radiant fluxes. The *MLR* profiles of AN/H_2SO_4 were in a shape of a narrow symmetry gauss curve, similar to the profiles of pure AN in Fig. 2. However, the *MLR* curves in Fig. 3 (f) were in a dissymmetric shape with much sharper *MLR* peaks. Since the *MLR* evolution profiles were determined by the pyrolysis reaction mechanism of samples, these curve shapes also indicated the different catalytic effects of CuO and H_2SO_4 on the pyrolysis of AN. Further analyses of their mechanisms are presented in Section 3.3.

3.3. Pyrolysis structure and mechanism analysis

The four-stage evolution characteristic of *MLR*s was caused by both temperature and mass concentration gradients inside the samples, which could be very complicated. Izato et al. [40] proposed a qualitative combustion wave structure model for AN mixed with carbon. Their model was adapted in this paper to explain the pyrolysis behavior of AN under thermal radiation scenario.

When exposed to radiation, the entire AN samples could be

qualitatively divided into four zones according to the spatial positions, dominating physical states and chemical reactions, as shown in Fig. 4 (a). The first zone on the sample bottom refers to the unreacted samples. Above zone 1 is the second zone where the dominating behavior of samples include melting, thermal decomposition and gas evolution. Most of the samples in zone 1 and zone 2 are of condensed phase (liquid or solid). The third zone above zone 2 corresponds to the preheating and diffusion of generated gases. And the zone 4 is mainly related to the combustion and evolution of gases. Please note that this model presents a simplified illustration with assumption that, only the dominating state of sample component and major thermal behavior could determine the physical and chemical interactions among the four zones. In real fire scenario, zone 2 may also consist of gaseous components as they were continuously generated during thermal decomposition.

For samples with certain thickness, the evolution of reaction zones in the pyrolysis structure model was related to the primary thermal decomposition reactions in the condensed phases [40]. Previous researchers [1,8,41] have widely accepted that, the decomposition of AN could be explained by two kinds of mechanisms, the ionic reactions (with sample at 200 ~ 300 °C, low reaction rate) and radical reactions (with sample above 290 °C, high reaction rate). Since the temperature of AN surface under radiation was in the range of 200 ~ 500 °C [42,43], both ion reactions and radical reactions occurred in the reaction zones. The evolution of pyrolysis stages and corresponding decomposition pathways are as follows.

First, when AN was exposed to radiation, the thermal decomposition zone was created, in which AN on the top layer melted through R1 at about 170 °C [42,43]. The liquids continuously decomposed through ionic R2. Although this reaction was endothermic, the radiation from cone heater continuously provided energy and supported the further reactions of NH_3 and HNO_3 through R3 ~ R6 [40,41,44]. Among these reactions, acidic species such as ammonium ion, hydronium ion and nitric acid drastically increased the decomposition rate of AN, while some bases such as ammonia or water retarded the decomposition.

$$NH_4NO_3(s) \xrightarrow{\text{Melt}} NH_4NO_3(l) \quad \text{(R1)}$$

$$NH_4NO_3(l) \rightleftarrows NH_3 + HNO_3 \quad \text{(R2)}$$

$$HNO_3 + HNO_3 \rightleftarrows H_2ONO_2^+ + NO_3^- \quad \text{(R3)}$$

$$H_2ONO_2^+ \rightleftarrows NO_2^+ + H_2O(g) \quad \text{(R4)}$$

$$NO_2^+ + NH_3 \rightarrow [NH_3NO_2^+] \quad \text{(R5)}$$

$$[NH_3NO_2^+] \rightarrow N_2O(g) + H_3O^+ \quad \text{(R6)}$$

With the increase of temperature inside samples, the ionic mechanism was replaced by a series of radical reactions, releasing lots of heat energy. Followed by R2, the hemolysis of O-N bond in HNO_3 occurred by R7. The hemolysis of HNO_3 had very high activation energy and R7 was the rate-controlling step. After that, several high speed radical chain reactions occurred via R8 ~ R13 and generated gases [3,15,23,44]. These reactions primarily occurred in zone 2 and released a large amount of heat, which in turn preheated the zone 3. The formed gases also evolved from the zone 2 to zone 3 and zone 4, and was eventually released into the ventilation system.

$$HONO_2 \rightarrow HO\cdot + NO_2(g) \quad \text{(R7)}$$

$$HO\cdot + NH_3 \rightarrow H_2O\ (g) + NH_2\cdot \quad \text{(R8)}$$

$$NH_2\cdot + NO_2 \rightarrow NH_2NO_2 \quad \text{(R9)}$$

$$NH_2NO_2 \rightarrow N_2O\ (g) + H_2O\ (g) \quad \text{(R10)}$$

$$NH_3 \rightarrow H\cdot + NH_2\cdot \quad \text{(R11)}$$

$$NH_2\cdot + NH_2\cdot \rightarrow N_2H_4\cdot \quad \text{(R12)}$$

$$N_2H_4 \rightarrow N_2(g) + 2H_2(g) \quad \text{(R13)}$$

From above, the different dominating chemical reactions in the pyrolysis structure model contributed to the four-stage characteristics. However, the model in Fig. 4 (a) cannot indicate how the thermal behavior and sample status change with radiation time or with the pyrolysis stages. Therefore, this paper developed a Fig. 4 (b) consisting of four illustrations to explain the relation between reaction zones and *MLR*s stages. At stage I, most of AN did not react and the pyrolysis structure model was dominated by the zone 1. The *MLR* gradually increased due to the consumption of limited AN in zone 2. A small amount of gas was released through zone 3 and then zone 4 into the air. After a period of time, more and more AN melted by R1 and decomposed through R2. Since both reactions were endothermic, the heat energy from cone heater was absorbed into zone 2 to support the subsequent reactions, leading to the stage II. At this stage, zones 1 ~ 3 all exist in the pyrolysis structure model, and the *MLRs* of AN would not increase much. In stage III, the underlying materials absorbed more energy, and R7 ~ R13 were activated. The generated heat continuously supported the melting of the unreacted AN. With sufficient exothermic activity in the condensed phase, zone 2 dominantly controlled the pyrolysis structure

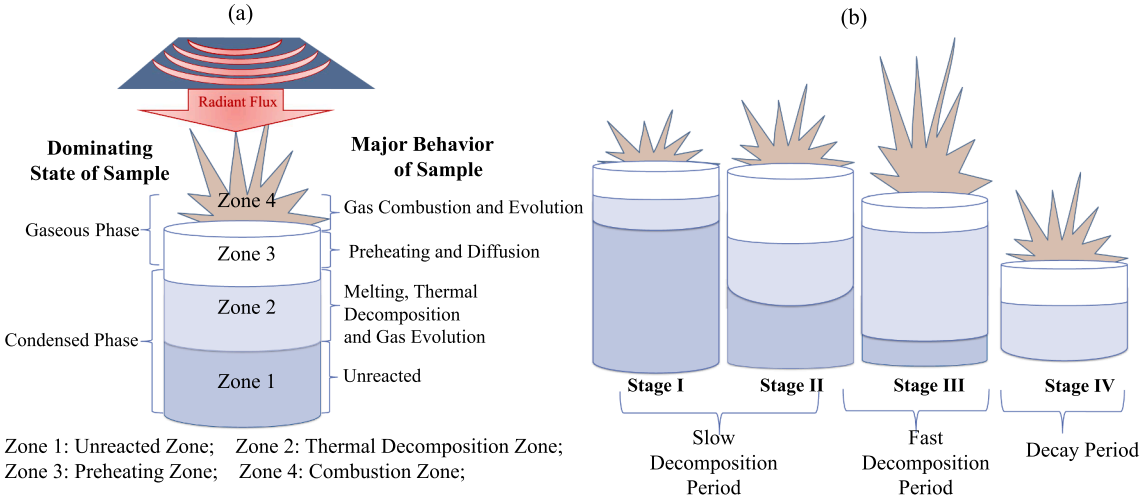

Fig. 4. (a) Illustration of the pyrolysis structure model of AN exposed to thermal radiation, adapted from [40]; (b) The pyrolysis structure model of AN in each pyrolysis stage.

model through noticeable reactions in both condensed-phase and gaseous phase. Combustible gases fed the heat transfer from the burning surface, and the pyrolysis continued by releasing a much larger amount of gases. Then the sample became thinner, the radiant energy on the top surface was smaller and the pyrolysis of AN started to decay through the stage IV.

The pyrolysis behavior of pure AN was determined by both reaction mechanisms and reaction zones. For the reaction mechanism of AN/CuO, both ion reactions and radical reactions have been proposed. A representative study by Sudhakar and Mathew [45] presented the reaction between CuO and AN through temperature resolved XRD pattern and IR spectral analysis. At the temperature of 55 ~ 245 °C, a solid-state reaction between AN and CuO took place by the interdiffusion of Cu^{2+} and H^{+} ions into and out of the AN crystal lattice, resulting in the formation of diammine copper (II) dinitrate solid solution ($[Cu(NH_3)_2](NO_3)_2$). The reaction pathway is presented as R14 [45].

$$2NH_4NO_3 + CuO \xrightarrow{\Delta} [Cu(NH_3)_2](NO_3)_2 + H_2 \quad (R14)$$

When temperature was above 245 °C, the solid solution decomposed while CuO remained the solid state. The reaction rate was controlled by radical reactions. To explore the interaction between CuO and AN, a GeminiSEM 500 was applied to capture the SEM picture of AN/CuO mixtures, as presented in Fig. 5 (a). The particle size of AN crystal (about 3 mm) was much larger than that of CuO powder (around 0.1 μm). Apart from some gaps (the black background), the surface of AN was largely encompassed by the CuO after mechanical mixing. Based on this, previous authors [25,46] proposed a surface absorption mechanism to describe the effects of CuO. The ammonia molecule could be retained on the surface of oxides in three possible ways [46], (i) hydrogen-bonding via one of its hydrogen atoms to a surface oxygen atom (or to the oxygen of a surface hydroxyl group), (ii) hydrogen-bonding via its nitrogen atom to the hydrogen of a surface hydroxyl group, and (iii) coordination to an electron-deficient metal atom (Lewis acid site). Therefore, CuO provided oxygen atom and copper metal atom to support these pathways through surface absorption [25]. Besides, there is a fourth mechanism shown by the illustration (iv), that the dissociation of ammonia with the formation of surface NH_2 and OH species as well as the transfer of protons to ammonia molecular from Bronsted sites to generate absorbed NH_4^+ ions [46]. Adapted from above analysis, a Fig. 5 (b) is plotted to show the possible absorption behavior of CuO on AN's surface. Relating these pathways to the aforementioned radical mechanism, the free radical HO· was mainly generated by R7, and the NH_2· was formed through R8 and R11. Based on the Le Chatelier's principle, the equilibriums of R2, R7, R8 and R11 were primarily displaced to the right, and in turn catalyzed the dissociation of AN. Since CuO did not decompose during the absorption process, it would remain in the final residue.

Relating the adsorption pathways to the pyrolysis structure model of AN/CuO, it could be found that under low radiant flux (with temperature less than 245 °C), the ion mechanism, i.e. the R14 mainly controlled the pyrolysis process by impacting zone 2. With increase of radiant flux, the CuO surface reactions could promote the breakdown of NH_3 into smaller species. Therefore, the dissociation products were removed at a comparatively faster rate by supporting the reactions in zone 2. The adsorbed NH_3 on the CuO surface also continuously accelerated the generation of other gaseous products, and thus promoted the reactions in zone 3 and zone 4. Besides, the CuO's adsorption behavior could be influenced by the heat energy absorbed, and the parallel-reaction mechanism may get converted into a parallel-consecutive-reaction mechanism at elevated temperature [25], causing the sharper *MLR* peaks at higher radiant fluxes. The adsorption mechanism provides important insights for chemical processes that involve CuO and AN, especially in the ammonia selective catalytic reduction of nitrogen oxide. Comparing to micro scale, CuO in nanoscale is more likely to cause significant catalytic effects if AN is wrapped by CuO as much as possible. Therefore, material designers can apply nanostructured CuO to AN by improving the absorption effects, thus improving the burning rates of catalyzed composite solid propellants [47].

For the effects of H_2SO_4, Sun et al. [23] have explained its catalytic mechanism through the ion reaction mechanism. H_2SO_4 reacted with AN by replacing the NO_3^- ion with HSO_4^- and generated nitric acid, as presented in R15. The generated HNO_3 and NH_4HSO_4 further decomposed through R16 into H_2SO_4. These two reactions in turn enhanced the decomposition of AN by accelerating the reactions of pure AN, i.e. the R3 ~ R6. Obviously, H_2SO_4 did not change the major reaction steps, but only increased the reaction rate by continuously generating nitric acid. It was the generated acid that contributed to the rapid decomposition of AN via R7 ~ R13. Therefore, similar to pure AN, the evolution of *MLRs* for AN/H_2SO_4 mixtures still consisted of four stages. When it comes to radical reactions at elevated temperature, the catalytic effects of H_2SO_4 could be represented by R15 and R16.

$$NH_4NO_3 + H_2SO_4 \rightarrow NH_4HSO_4 + HNO_3 \quad (15)$$

$$NH_4HSO_4 \rightarrow NH_3 + H_2SO_4 \quad (16)$$

3.4. Discussions and implications for emergency response

Previous studies at milligram scale generally indicate a single pyrolysis stage of AN [1,13,14] in accordance to one set of kinetics and thermodynamics. The derived kinetic parameters, as well as the physical and chemical mechanisms, allow us to obtain pyrolysis, gasification and combustion models that reproduce the best possible reality. However, there are several restrictions on the use of such kinetic parameters for real cases, which normally suffer much higher heating rates than the possible heating rates in a TGA. Besides, the non-dimensional heating condition cannot fully represent the heated status of AN or mixtures in

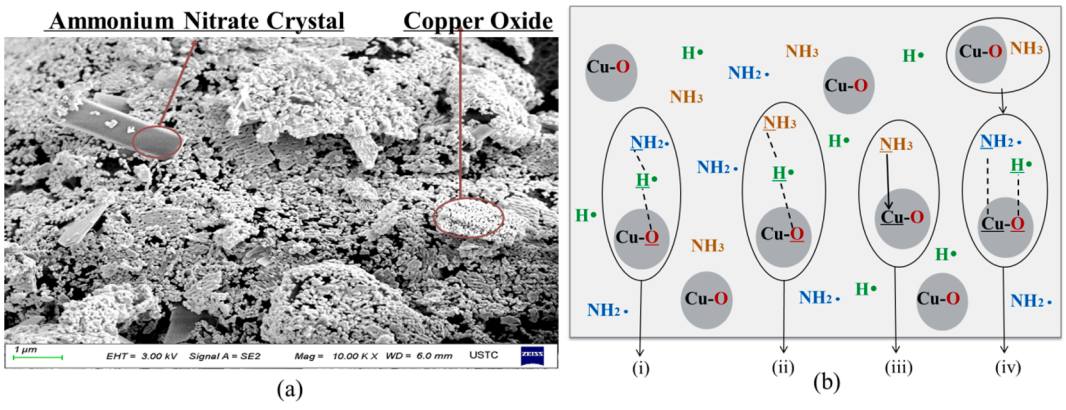

Fig. 5. (a) The SEM picture of AN/CuO mixture; (b) The adsorption pathways of ammonia and radicals on CuO surface [25,46].

real fire [21]. Through fire radiation dominated bench scale experiments, this study has proved two facts. Firstly, the pyrolysis stages of AN accumulated in bench scale differ from that in milligram scale. Secondly, the physical and chemical phenomena that occur in the bench scale pyrolysis can be explained by existing mechanisms through a pyrolysis structure. Therefore, to obtain the pyrolysis, gasification and combustion models for AN and related mixtures, more sophisticated experimental planning should be proposed considering the differences between milligram scale and bench scale, and to develop multiple sets of kinetics for pyrolysis of AN in real fire.

Summarizing the evolutions of *MLR*s with time (t) at different stages, this paper presents a qualitative illustration of the burning timelines of AN, AN/CuO and AN/H_2SO_4 under radiation, as plotted in Fig. 6. It consists of five curves, indicating the evolvement of pyrolysis stages of AN under different scenarios. The shaded area marked as curve 1 refers to the burning timeline of pure AN. The timeline consisted of melting, slow decomposition period, fast decomposition period and decay period, respectively. Depending on the change of sample composition or the exposed fire scenario (radiant flux), four additional timelines are obtained. The increases of sample mass can improve the *MLR*s at each stage, but will not significantly shorten the time of each stage (curve 2). When increasing radiant flux (curve 3), the *MLR* increases while the time of each stage reduces. The involvement of H_2SO_4 has similar effects (curve 4). Besides, the *MLR*s of curve 1 ~ 4 all share the four-stage characteristics, i.e. slowly increase, being stable, rapid increase and decay. In the fast decomposition period, these *MLR* curves approximately have a symmetric Gaussian shape. However, the involvement of CuO (curve 5) will change the four-stage pattern into three. The *MLR* profile in the fast decomposition period for AN/CuO mixtures is unsymmetrical with a sharper peak.

Fig. 6 qualitatively describes the potential hazards of AN under varied fire scenarios, but the ultimate goal of conducting these radiation experiments is to provide useful insights for emergency response and fire safety control in case AN is exposed to external fire. As mentioned in Section 1, pure AN is not the cause of fire and explosion accidents and yet the uncontrolled external fire provides heat energy to support the melting and decomposition of AN. The generated intermediate chemicals with strong oxidation capacity will enhance the reactions and accelerate the pyrolysis process. Therefore, to prevent AN related fire and explosion accidents, the best strategy is to isolate AN from any potential fire sources. Babrauskas [15] proposed two actions, the adoption of formulations to reduce the possibility of uncontrolled fire and explosions; and the application of building safety measures to provide assurance against uncontrolled fires. Although these safety strategies could solve the problem from the origin, disasters still continue to occur as such strategies are not easy to be implemented presently. When both actions fail and AN is exposed to external fire, necessary steps

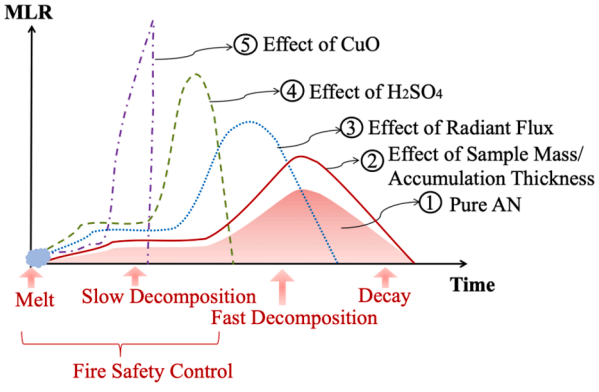

Fig. 6. Illustration of burning timelines of AN under thermal radiation (curve 1), and effects of sample mass (curve 2), radiant flux (curve 3), H_2SO_4 (curve 4) and CuO (curve 5) on the burning timelines.

should be taken to prevent the evolution of pyrolysis from slow decomposition to fast decomposition. Through the plots in Fig. 2 ~ 3 as well as the datasets presented in Table 2, this paper qualitatively identifies the pyrolysis stage evolution of AN, and quantitatively captures its pyrolysis characteristics. Regarding the time required for emergency response actions, further analyses were performed to explore the potential patterns among these datasets.

The changes of (a) time and (b) *MLR* of slow decomposition, fast decomposition and decay under different radiant fluxes are presented in Fig. 7. For comparison, it only covers the results of pure AN with 30 g, AN mixed with 5 wt% CuO and AN mixed with 6 wt% H_2SO_4. The numbers on the x-axis refer to the three heat fluxes, i.e. external fire with different radiation intensities. Generally, with an increase in heat flux, the time of slow decomposition (i.e. t_{II}), fast decomposition (i.e. t_{III}) and decay (i.e. t_{end}) all reduces, while the *MLR*s of the first two stages increase. The increase rate indicates the sensitivities of sample to heat flux. Among the nine curves in Fig. 7 (a), curve 3 is the most sensitive one, followed by curve 1, 2 and 6. In Fig. 7 (b), curve 6 has the largest increase rate, followed by curve 3 and 4. This indicates that the increase of radiant flux mainly acts on the pyrolysis in the fast decomposition and decay period, rather than the slow decomposition period. On the other hand, the changes between 25 and 35 kW m^{-2} is more significant than that between 35 and 50 kW m^{-2}, although the former has a smaller gradient (10 kW m^{-2}). For the data distribution of all cases shown in Fig. 8, it indicates that the values of MLR_I and MLR_{II} are very close and generally less than 0.05 g s^{-1}, but the MLR_{max} is much higher. The region of t_{II} is approximately within the region of 100 ~ 300 s. Since the fundamental safety requirement is to prevent the transition of slow decomposition to fast decomposition, primary fire control strategy for AN in bulk must be taken before the averaged t_{II} in Fig. 8.

The reported results of Fig. 8 provide important technological implications for thermal safety control. There are two possible ways to prevent AN's fire-induced domino effect, prevention of the uncertain event, and intervention of the deterministic events. The dramatic consequence of Tianjin Port accident was largely due to the failed intervention of deterministic events. According to the official accident investigation report, the first fire (the uncertain event) occurred at 22:51:46. No effective detecting or firefighting strategies were taken since then, leading to the subsequent deterministic events among which the first explosions occurred at 23:34:06. AN continuously pyrolyzed within 42 min, with no sensitive fire detecting systems to timely identify the slow decomposition period, and there was no firefighting to isolate AN from the fire before it evolved into fast decomposition. Learning from Fig. 8, the consequence could be less severe if AN was isolated from external fire within the "Fire Safety Control" zone. Note that such zone involves both AN and several mixtures. For pure AN exposed to fire, the minimum time for t_{II} is 117 s at 50 kW m^{-2}. This time should be corrected with uncertainties and errors before making any fire safety plans. The uncertainty could be attributed to the cone heater [38] with error margin of 10%. In an ideal two-dimension scenario, the pyrolysis stage transition time of pure AN should not be influenced by sample mass. Therefore we calculated the standard deviation of t_{II} for pure AN with different masses under 50 kW m^{-2} (No. 13 ~ 15), and corrected the t_{II}. The calculated standard deviation is 48 s, in accordance to an error of 28%. Combining the two percentages, the corrected time before fast decomposition is about 75 s. Based on this time, researchers can estimate the fire detection time for performance-based fire protection design, and determine the required safety egress time [48]. For example, since AN accidents are caused by external fire, radiant energy-sensing fire detectors can be applied in warehouses that store AN, to recognize the fire signals and send information to firefighting devices before AN reaches the fast decomposition period.

However, it should be noted that the *MLR*s and time of each pyrolysis stage could be influenced by radiant flux, sample mass, and both proportions and types of additives. The estimated time of 75 s in this paper is only applicable to the particular sample composites, i.e. pure AN, AN

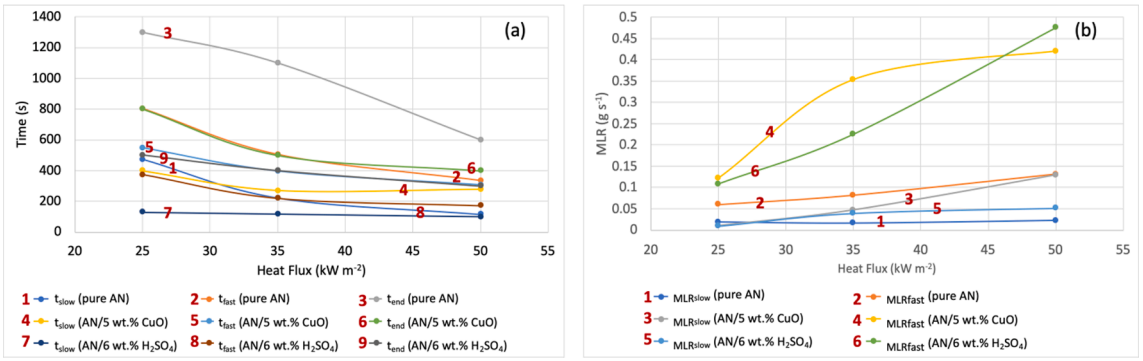

Fig. 7. The changes of (a) time and (b) *MLR* of slow decomposition (subscript, slow) and fast decomposition (subscript, fast) periods as well as (a) time of decay period (subscript, end) under different heat fluxes. The sample mass of AN is 30 g.

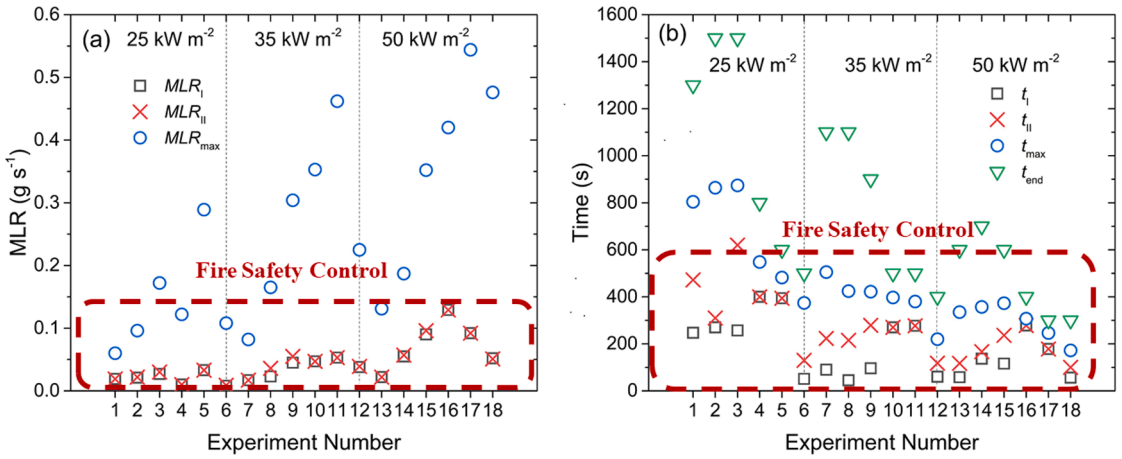

Fig. 8. The distribution of (a) *MLR*s and (b) time of each pyrolysis stage for AN, AN/CuO and AN/H_2SO_4 under radiant flux of 25 kW m^{-2} (1 ~ 6), 35 kW m^{-2} (7 ~ 12) and 5 kW m^{-2} (13 ~ 18).

mixed with 10 wt% CuO or less, and AN contaminated by 6 wt% H_2SO_4 or less with radiant flux less than 50 kW m^{-2}. The emergency response time must be shorter if AN was exposed to higher radiant flux or AN was mixed with either CuO or H_2SO_4 in larger proportions, or when AN is stored in confined spaces. Moreover, the potential additives or containments of AN could be much more complicated in industrial accidents. Both experimental and theoretical studies of additional scenarios are necessary in future.

4. Conclusions

The uncontrolled external fire has been proved by literatures to be the primary cause of dramatic explosion accidents of ammonium nitrate in industry, but limited studies have been conducted to investigate the behavior of ammonium nitrate in fire. By simulating typical fire scenarios, this paper conducted a series of thermal radiation experiments through an ISO 5660 cone heater to explore the pyrolysis behavior of ammonium nitrate, ammonium nitrate/copper oxide and ammonium nitrate/sulfuric acid. Through in-depth analysis of the mass loss, a four-stage characteristic process (from stage I to stage IV) in accordance to three dominating pyrolysis periods (slow decomposition, fast decomposition and decay) was identified. Data of both mass loss rate and time at each stage were collected. The increase of accumulation mass did not significantly change the stage transition time, and yet higher radiant flux mainly accelerated the reaction rate in fast decomposition period. Four pyrolysis structure models were established to relate the combustion behavior at different pyrolysis stages. Besides, it was found that the involvement of copper oxide and sulfuric acid accelerated the pyrolysis rate of ammonium nitrate through different catalytic mechanisms. Sulfuric acid did not change the four-stage characteristic process, but enhanced the decomposition reaction rate of each stage by generating more nitric acid. Copper oxide catalyzed the pyrolysis of ammonium nitrate by merging the stage I and II and generating a sharp and unsymmetrical mass loss rate profile in the fast decomposition period. Five burning timelines were developed to qualitatively describe the pyrolysis behavior of ammonium nitrate under different scenarios. The safety time for fire safety control depended on both radiant flux and sample compositions. An emergency response time of 75 s is recommended to isolate materials from external fire, if samples including pure ammonium nitrate, ammonium nitrate mixed with 10 wt% copper oxide or less, and ammonium nitrate contaminated by 6 wt% sulfuric acid or less are exposed to external fire with radiant flux of 50 kW m^{-2} at most.

Declaration of Competing Interest

The authors declare that they have no known competing financial interests or personal relationships that could have appeared to influence the work reported in this paper.

Acknowledgement

This research was supported by the National Natural Science Foundation of China (NSFC, Grant 51976209, 51806208) and the Public Welfare Science and Technology Plan of Ningbo City (2019C50013). The authors greatly acknowledge these supports.

References

[1] V. Babrauskas, D. Leggett, Thermal decomposition of ammonium nitrate, Fire Mater. 44 (2020) 250–268. https://doi:10.1002/fam.2797.

[2] X. Baraza, A. Pey, J. Giménez, The self-sustaining decomposition of ammonium nitrate fertiliser: Case study, Escombreras valley, Spain, J. Hazard. Mater. 387 (2020), 121674, https://doi.org/10.1016/j.jhazmat.2019.121674.

[3] J. Jos, S. Mathew, Ammonium Nitrate as an Eco-Friendly Oxidizer for Composite Solid Propellants: Promises and Challenges, Crit. Rev. Solid State Mater. Sci. 42 (2017) 470–498. https://doi:10.1080/10408436.2016.1244642.

[4] C. Oommen, S.R. Jain, Ammonium nitrate: a promising rocket propellant oxidizer, J. Hazard. Mater. 67 (1999) 253–281, https://doi.org/10.1016/S0304-3894(99)00039-4.

[5] G. Marlair, M.-A.A. Kordek, Safety and security issues relating to low capacity storage of AN-based fertilizers, J. Hazard. Mater. 123 (2005) 13–28. https://doi:10.1016/j.jhazmat.2005.03.028.

[6] S. Chaturvedi, P.N. Dave, Review on Thermal Decomposition of Ammonium Nitrate, J. Energ. Mater. 31 (2013) 1–26. https://doi:10.1080/07370652.2011.573523.

[7] M. Yang, X. Chen, Y. Wang, B. Yuan, Y. Niu, Y. Zhang, R. Liao, Z. Zhang, Comparative evaluation of thermal decomposition behavior and thermal stability of powdered ammonium nitrate under different atmosphere conditions, J. Hazard. Mater. 337 (2017) 10–19. https://doi:10.1016/j. jhazmat.2017.04.063.

[8] J.C. Oxley, J.L. Smith, E. Rogers, M. Yu, Ammonium nitrate: thermal stability and explosivity modifiers, Thermochim. Acta. 384 (2002) 23–45, https://doi.org/10.1016/S0040-6031(01)00775-4.

[9] R. Gunawan, D. Zhang, Thermal stability and kinetics of decomposition of ammonium nitrate in the presence of pyrite, J. Hazard. Mater. 165 (2009) 751–758. https://doi:10.1016/j. jhazmat.2008.10.054.

[10] K. Fujisato, H. Habu, A. Miyake, K. Hori, Thermal decomposition of ammonium nitrate modeling of thermal dissociation in thermal analysis, Sci Technol Energ Mater. 75 (2014) 28–36, https://doi.org/10.1016/j.jhazmat.2017.04.063.

[11] V. P. Sinditskii, V.Y. Egorshev, A.I. Levshenkov, V. V. Serushkin, Ammonium nitrate: Combustion mechanism and the role of additives, in: Propellants, Explos. Pyrotech., John Wiley & Sons, Ltd, 2005: pp. 269–280. https://doi:10.1002/prep.200500017.

[12] Z. Han, S. Sachdeva, M.I. Papadaki, M.S. Mannan, Ammonium nitrate thermal decomposition with additives, J. Loss Prev. Process Ind. 35 (2015) 307–315. https://doi:10.1016/J.JLP.2014.10.011.

[13] H.Q. Cao, Q.L. Duan, H. Chai, X.X. Li, J.H. Sun, Experimental study of the effect of typical halides on pyrolysis of ammonium nitrate using model reconstruction, J. Hazard. Mater. 384 (2020), 121297, https://doi.org/10.1016/j.jhazmat.2019.121297.

[14] H.Q. Cao, L. Jiang, Q.L. Duan, D. Zhang, H.D. Chen, J.H. Sun, An experimental and theoretical study of optimized selection and model reconstruction for ammonium nitrate pyrolysis, J. Hazard. Mater. 364 (2019) 539–547, https://doi.org/10.1016/j.jhazmat.2018.10.048.

[15] V. Babrauskas, Explosions of ammonium nitrate fertilizer in storage or transportation are preventable accidents, J. Hazard. Mater. 304 (2016) 134–149. https://doi:10.1016/j.jhazmat.2015.10.040.

[16] Q. Chen, M. Wood, J. Zhao, Case study of the Tianjin accident: Application of barrier and systems analysis to understand challenges to industry loss prevention in emerging economies, Process Saf. Environ. Prot. 131 (2019) 178–188, https://doi.org/10.1016/j.psep.2019.08.028.

[17] F. Gui, J. Wang, M. Yan, G. Fu, J. Wang, M. Yan, F. Gui, J. Wang, M. Yan, G. Fu, J. Wang, M. Yan, Anatomy of Tianjin Port fire and explosion: Process and causes, Process Saf. Prog. 35 (2016) 216–220. https://doi:10.1002/prs.11837.

[18] L. Ding, J. Ji, F. Khan, Combining uncertainty reasoning and deterministic modeling for risk analysis of fire-induced domino effects, Saf. Sci. 129 (2020), 104802, https://doi.org/10.1016/j.ssci.2020.104802.

[19] J. Ji, Q. Tong, F. Khan, M. Dadashzadeh, R. Abbassi, Risk-Based Domino Effect Analysis for Fire and Explosion Accidents Considering Uncertainty in Processing Facilities, Ind. Eng. Chem. Res. 57 (2018) 3990–4006. doi:10.1021/acs.iecr.8b00103.

[20] L. Ding, F. Khan, J. Ji, A novel approach for domino effects modeling and risk analysis based on synergistic effect and accident evidence, Reliab. Eng. Syst. Saf. 203 (2020), 107109, https://doi.org/10.1016/j.ress.2020.107109.

[21] Q. Sun, L. Jiang, M. Li, J. Sun, Assessment on thermal hazards of reactive chemicals in industry: State of the Art and perspectives, Prog. Energy Combust. Sci. 78 (2020), 100832, https://doi.org/10.1016/j.pecs.2020.100832.

[22] Z. Han, H.J. Pasman, M.S. Mannan, Extinguishing fires involving ammonium nitrate stock with water: Possible complications, J. Fire Sci. 35 (2017) 457–483, https://doi.org/10.1177/0734904117735264.

[23] J. Sun, Z. Sun, Q. Wang, H. Ding, T. Wang, C. Jiang, Catalytic effects of inorganic acids on the decomposition of ammonium nitrate, J. Hazard. Mater. 127 (2005) 204–210. https://doi:10.1016/j.jhazmat.2005.07.028.

[24] Z. Xu, G. Xu, X. Fu, Q. Wang, The mechanism of nano-CuO and CuFe2o4 catalyzed thermal decomposition of ammonium nitrate, Nanomater. Nanotechnol. 6 (2016) 184798041668169. https://doi:10.1177/1847980416681699.

[25] A.A. Vargeese, K. Muralidharan, Kinetics and mechanism of hydrothermally prepared copper oxide nanorod catalyzed decomposition of ammonium nitrate, Appl. Catal. A Gen. 447–448 (2012) 171–177, https://doi.org/10.1016/j.apcata.2012.09.027.

[26] K. Kajiyama, Y. Izato, A. Miyake, Thermal characteristics of ammonium nitrate, carbon, and copper(II) oxide mixtures, J. Therm. Anal. Calorim. 113 (2013) 1475–1480. https://doi:10.1007/s10973-013-3201-5.

[27] B. Schartel, M. Bartholmai, U. Knoll, Some comments on the use of cone calorimeter data, Polym. Degrad. Stab. 88 (2005) 540–547, https://doi.org/10.1016/j.polymdegradstab.2004.12.016.

[28] I.S.O. 5660-1, Reaction-to-fire tests-Heat release, smoke production and mass loss rate-Part 1: heat release rate (cone calorimeter method), Geneva, Switz. Int. Stand. Organ. (2002).

[29] H.S. Ding, H. Jiang, Self-heating co-pyrolysis of excessive activated sludge with waste biomass: Energy balance and sludge reduction, Bioresour. Technol. 133 (2013) 16–22. https://doi:10.1016/j.biortech.2013.01.090.

[30] R. Emberley, T. Do, J. Yim, J.L. Torero, Critical heat flux and mass loss rate for extinction of flaming combustion of timber, Fire Saf. J. 91 (2017) 252–258, https://doi.org/10.1016/j.firesaf.2017.03.008.

[31] O. Grexa, H. Lübke, Flammability parameters of wood tested on a cone calorimeter, Polym. Degrad. Stab. 74 (2001) 427–432, https://doi.org/10.1016/S0141-3910(01)00181-1.

[32] Y. Ding, S.I. Stoliarov, R.H. Kraemer, Pyrolysis model development for a polymeric material containing multiple flame retardants: Relationship between heat release rate and material composition, Combust. Flame. 202 (2019) 43–57, https://doi.org/10.1016/j.combustflame.2019.01.003.

[33] M.B. McKinnon, Y. Ding, S.I. Stoliarov, S. Crowley, R.E. Lyon, Pyrolysis model for a carbon fiber/epoxy structural aerospace composite, J. Fire Sci. 35 (2017) 36–61. https://doi:10.1177/0734904116679422.

[34] B.T. Rhodes, J.G. Quintiere, Burning rate and flame heat flux for PMMA in a cone calorimeter, Fire Saf. J. 26 (1996) 221–240, https://doi.org/10.1016/S0379-7112(96)00025-2.

[35] B. Li, A study of thermal degradation and decomposition of rigid poly (vinyl chloride) with metal oxides using thermogravimetry and cone calorimetry, Polym. Degrad. Stab. 68 (2000) 197–204, https://doi.org/10.1016/S0141-3910(00)00002-1.

[36] J. Luche, T. Rogaume, F. Richard, E. Guillaume, Characterization of thermal properties and analysis of combustion behavior of PMMA in a cone calorimeter, Fire Saf. J. 46 (2011) 451–461, https://doi.org/10.1016/j.firesaf.2011.07.005.

[37] V. Babrauskas, The cone calorimeter, in: SFPE Handb. Fire Prot. Eng., Springer, 2016: pp. 952–980.

[38] G. Wypych, Testing Methods in Filled Systems, in: Handbook of Fillers (Fourth Edition), Elsevier, 2016: pp. 627–664. doi:10.1016/B978-1-895198-91-1.50016-6.

[39] J.E.J. Staggs, Savitzky-Golay smoothing and numerical differentiation of cone calorimeter mass data, Fire Saf. J. 40 (2005) 493–505, https://doi.org/10.1016/j.firesaf.2005.05.002.

[40] Y.I. Izato, A. Miyake, S. Date, Combustion characteristics of ammonium nitrate and carbon mixtures based on a thermal decomposition mechanism, Propellants, Explos. Pyrotech. 38 (2013) 129–135. https://doi:10.1002/prep.201100106.

[41] K.R. Brower, J.C. Oxley, M. Tewari, Evidence for homolytic decomposition of ammonium nitrate at high temperature, J. Phys. Chem. 93 (1989) 4029–4033, https://doi.org/10.1021/j100347a033.

[42] A. Miyake, Y. Izato, Thermal Decomposition Behaviors of Ammonium Nitrate and Carbon Mixtures, Int. J. Energ. Mater. Chem. Propuls. 9 (2010) 523–531. https://doi:10.1615/IntJEnergeticMaterialsChemProp.2011001429.

[43] Y. Wada, K. Hori, M. Arai, Combustion mechanism of mixtures of guanidine nitrate, ammonium nitrate, and basic copper nitrate, Sci Technol Energ Mater. 71 (2010) 83–87.

[44] Y. Izato, A. Miyake, Thermal decomposition of molten ammonium nitrate (AN), J. Therm. Anal. Calorim. 122 (2015) 595–600. https://doi:10.1007/s10973-015-4762-2.

[45] A.O.R. Sudhakar, S. Mathew, Thermal behaviour of CuO doped phase-stabilised ammonium nitrate, Thermochim. Acta. 451 (2006) 5–9, https://doi.org/10.1016/j.tca.2006.08.013.

[46] A.A. Tsyganenko, D.V. Pozdnyakov, V.N. Filimonov, Infrared study of surface species arising from ammonia adsorption on oxide surfaces, J. Mol. Struct. 29 (1975) 299–318, https://doi.org/10.1016/0022-2860(75)85038-1.

[47] K.V. Suresh Babua, P.K. Raju, C.R. Thomas, A.S. Hamed, K.N. Ninan, Studies on composite solid propellant with tri-modal ammonium perchlorate containing an ultrafine fraction, Defence Tech. 13 (2017) (2017) 239–245, https://doi.org/10.1016/j.dt.2017.06.001.

[48] Q. Li, Estimation of fire detection time, in: Procedia Eng., 2011. doi:10.1016/j.proeng.2011.04.652.